

Competing exchange interactions on the verge of a metal-insulator transition in the two-dimensional spiral magnet $\text{Sr}_3\text{Fe}_2\text{O}_7$

J.-H. Kim,¹ Anil Jain,^{1,2} M. Reehuis,³ G. Khaliullin,¹ D. C. Peets,¹ C. Ulrich,^{1,4,5} J. T. Park,⁶ E. Faulhaber,⁶ A. Hoser,³ H. C. Walker,⁷ D. T. Adroja,^{7,8} A. C. Walters,¹ D. S. Inosov,^{1,9} A. Maljuk,^{1,10} and B. Keimer^{1,*}

¹*Max-Planck-Institut für Festkörperforschung, D-70569 Stuttgart, Germany*

²*Solid State Physics Division, Bhabha Atomic Research Centre, Mumbai 400085, India*

³*Helmholtz-Zentrum Berlin für Materialien und Energie, D-14109 Berlin, Germany*

⁴*School of Physics, University of New South Wales, Sydney, NSW 2052, Australia*

⁵*Australian Nuclear Science and Technology Organisation, Lucas Heights, NSW 2234, Australia*

⁶*Forschungszentrum für Neutronenphysik und Technik, Heinz Maier-Leibnitz (FRM-II), D-85748 Garching, Germany*

⁷*ISIS Facility, STFC, Rutherford Appleton Laboratory,*

Chilton, Didcot, Oxfordshire, OX11-0QX, United Kingdom

⁸*Physics Department, Highly Correlated Matter Research Group,*

University of Johannesburg, PO Box 524, Auckland Park 2006, South Africa

⁹*Institut für Festkörperphysik, TU Dresden, D-01069 Dresden, Germany*

¹⁰*Leibniz Institut für Festkörper- und Werkstoffforschung, D-01171 Dresden, Germany*

(Dated: September 19, 2014)

We report a neutron scattering study of the magnetic order and dynamics of the bilayer perovskite $\text{Sr}_3\text{Fe}_2\text{O}_7$, which exhibits a temperature-driven metal-insulator transition at 340 K. We show that the Fe^{4+} moments adopt incommensurate spiral order below $T_N = 115$ K and provide a comprehensive description of the corresponding spin wave excitations. The observed magnetic order and excitation spectra can be well understood in terms of an effective spin Hamiltonian with interactions ranging up to third nearest-neighbor pairs. The results indicate that the helical magnetism in $\text{Sr}_3\text{Fe}_2\text{O}_7$ results from competition between ferromagnetic double-exchange and antiferromagnetic superexchange interactions whose strengths become comparable near the metal-insulator transition. They thus confirm a decades-old theoretical prediction and provide a firm experimental basis for models of magnetic correlations in strongly correlated metals.

PACS numbers: 28.20.Cz, 75.50.Ee, 75.30.Ds

Following theoretical progress including the development of the dynamical mean-field theory [1], the description of correlation-driven metal-insulator transitions (MITs) has recently been rapidly advancing, but realistic calculations of magnetic correlations near MITs remain a formidable challenge. Manganese oxides have served as prominent model materials for research on magnetism in proximity to MITs. Whereas localized spins in insulating manganates interact via (predominantly antiferromagnetic) superexchange interactions mediated by high-energy virtual excitations of the Mn d -electrons, ferromagnetic double-exchange interactions mediated by itinerant electrons dominate in their metallic counterparts. In terms of dynamical mean field theory, superexchange and double-exchange interactions originate in high-energy incoherent (“Hubbard-like”) and narrow quasiparticle (“Kondo-like”) bands, respectively [2]. According to a long-standing prediction [3], competition between these antagonistic exchange interactions generates non-collinear magnetic structures in the vicinity of MITs. Unfortunately, disorder-induced electronic phase separation near MITs [4] has thus far largely precluded experimental tests of this prediction in manganates and other transition metal oxides (TMOs).

Non-collinear magnetism has been observed in a small number of disorder-free model materials (including

NdNiO_3 [5] and CaFeO_3 [6]) that exhibit temperature-driven MITs, and in TMO superlattices where MITs can be driven by adjusting the doping level [7] or electronic dimensionality [8] without introducing disorder. Following the original prediction [3], these structures have been discussed on a qualitative level in terms of competing superexchange and double-exchange interactions [2, 7, 9], but alternative interpretations have also been proposed. In particular, it was pointed out that double exchange alone can generate spiral magnetism in TMOs with metal ions in high oxidation states, where the usual charge transfer between metal d - and oxygen p -states is at least partially reversed [10, 11]. Both models differ in their predictions for the magnitudes and spatial range of the exchange coupling between electron spins on different lattice sites. In principle, these parameters can be extracted from the spin wave dispersions measured by inelastic magnetic neutron scattering (INS). To the best of our knowledge, however, such measurements have not been reported for stoichiometric model materials, because crystals of sufficient size and quality have not been available.

In order to guide and test theoretical concepts of magnetic order near MITs, we have used neutron scattering to investigate the magnetic structure and dynamics of fully oxygenated $\text{Sr}_3\text{Fe}_2\text{O}_7$, a stoichiometric compound built up of bilayers of FeO_6 octahedra that was recently found to

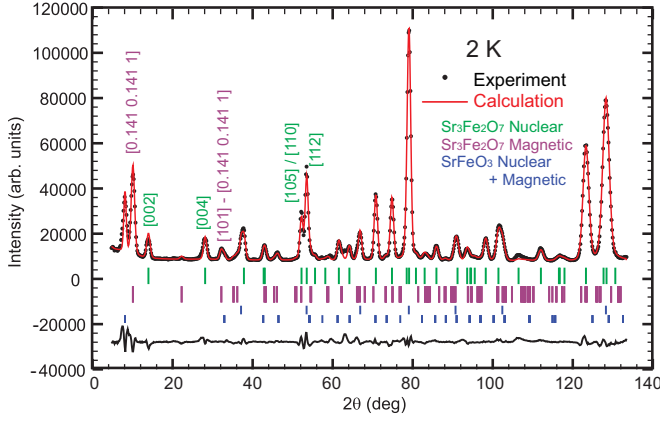


FIG. 1. (Color online) Neutron powder diffraction data of $\text{Sr}_3\text{Fe}_2\text{O}_7$ at 2 K. The helical spin modulation vector in $\text{Sr}_3\text{Fe}_2\text{O}_7$ was found to be $\vec{k} = [0.141 \ 0.141 \ 1]$ (in the tetragonal setting). The upper symbols and line represent experimental data and calculated results, respectively. A small amount of SrFeO_3 ($T_N = 133$ K) in our powder sample manifests its helical magnetic phase with $\vec{k} = [0.129, 0.129, 0.129]$, consistent with fully-oxygenated SrFeO_3 [23]. Upper, middle, and bottom bars indicate the calculated positions of $\text{Sr}_3\text{Fe}_2\text{O}_7$ nuclear, $\text{Sr}_3\text{Fe}_2\text{O}_7$ magnetic, and SrFeO_3 reflections, respectively, and the bottom line is a residual.

undergo a continuous transition from a high-temperature metallic to a low-temperature insulating phase at temperature $T_{\text{MIT}} = 340$ K [12]. This material is based on Fe^{4+} ions (nominal electron configuration $3d^4$), which are isoelectronic to Mn^{3+} ($3d^4$) and closely analogous to Ru^{4+} ($4d^4$) ions in two extensively studied families of manganates and ruthenates, and it is isostructural to the compounds $\text{La}_{2-x}\text{Sr}_x\text{Mn}_2\text{O}_7$ and $\text{Sr}_3\text{Ru}_2\text{O}_7$ that are well known for their magnetoresistive properties [13] and electronic liquid-crystal behavior [14], respectively. Despite these analogies, we find that below the Néel temperature, $T_N = 115$ K, $\text{Sr}_3\text{Fe}_2\text{O}_7$ exhibits a spiral state that has no analog in manganates or ruthenates. Unlike other model materials [5, 6], single crystals with quality and volume sufficient for INS measurements have been grown [12, 15]. We have thus been able to determine the spin wave dispersions and extract the exchange parameters, which compare favorably with models based on competing superexchange and double-exchange interactions [2]. In contrast, predictions based on double exchange alone [10] do not yield satisfactory agreement with the data. Our data thus quantitatively confirm the long-standing prediction of competing exchange interactions near MITs [3], and they establish $\text{Sr}_3\text{Fe}_2\text{O}_7$ as a two-dimensional model material for spiral magnetism, which has recently attracted considerable attention in the context of research on multiferroicity, topological excitations [16], and copper- and iron-based high-temperature superconductors [17–19].

The experiments were performed on a powder sample of weight 3 g, and on cylindrical single crystals of diame-

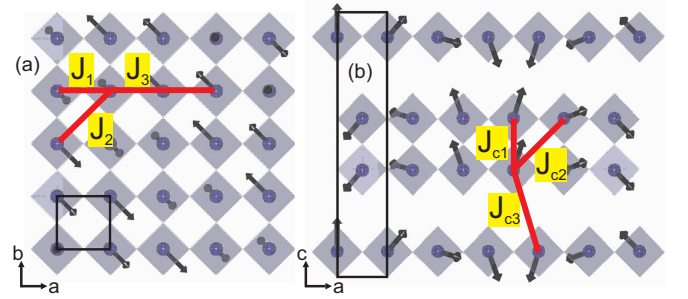


FIG. 2. (Color online) Helical magnetic structure of $\text{Sr}_3\text{Fe}_2\text{O}_7$ projected onto the (a) ab and (b) ac planes. The rectangle indicates the tetragonal unit cell. Spheres and octahedra represent the Fe ions and FeO_6 units, respectively. Arrows indicate the spin directions. Lines indicate the spin exchange couplings J included in the theoretical fits.

ter 5 mm and length 5 mm (5 cm) for elastic (inelastic) scattering. Their preparation and characterization are described in Refs. 12 and 15. All samples were characterized by neutron and x-ray diffraction, as described in Ref. 12. The magnetic structure was determined from single-crystal neutron diffraction data obtained on the E5 diffractometer (neutron wavelength $\lambda = 2.38$ Å), and powder data from the E6 diffractometer ($\lambda = 2.44$ Å) at BER-II (Helmholtz-Zentrum Berlin, Germany), respectively. INS experiments on a single crystal were carried out on neutron triple axis spectrometers (TAS) PANDA (cold TAS) and PUMA (thermal TAS) at the FRM-II (Munich, Germany) and direct-geometry time-of-flight (TOF) spectrometer MERLIN at the ISIS spallation neutron source (Didcot, UK). At PANDA, the momentum of the scattered neutrons was set to $k_f = 1.57$ Å $^{-1}$, and at PUMA, $k_f = 2.662$ Å $^{-1}$ was used. For the TOF measurements, the incident energy was 60 meV and the sample was mounted with the $(H\bar{H}L)$ scattering plane horizontal. The magnetic excitations throughout the Brillouin Zone in all symmetry directions were mapped out by rotating the crystal over 60° in steps of 1° about the vertical $[110]$ axis, starting from k_i along $[1\bar{1}0]$. The TOF data were transformed into units of energy and momentum transfer using the Horace software [20].

Figure 1 shows neutron powder diffraction data on $\text{Sr}_3\text{Fe}_2\text{O}_7$ at $T = 2$ K (well below T_N). They were refined using FullProf [21] based on the published tetragonal space group $I4/mmm$ (No. 139) with lattice parameters $a = b = 3.846(4)$ Å and $c = 20.234(2)$ Å (at $T = 390$ K). The best fit, with $R_F = \frac{\sum ||F_{\text{obs}}| - |F_{\text{calc}}||}{\sum |F_{\text{obs}}|} = 0.061$, implies that $\text{Sr}_3\text{Fe}_2\text{O}_7$ has an incommensurate magnetic propagation vector of $\vec{k} = [\xi \ \xi \ 1]$ with $\xi = 0.1416(3)$. In addition to the powder refinements, single-crystal neutron diffraction data measured at $T = 10$ K were refined with $R_B = \frac{\sum ||I_{\text{obs}}| - |I_{\text{calc}}||}{\sum |I_{\text{obs}}|} = 0.093$, based on 142 magnetic reflections (26 unique). The refinement results of the

powder (2 K) and single crystal (10 K) data are almost identical. The magnetic structure of $\text{Sr}_3\text{Fe}_2\text{O}_7$ obtained in this way is helical with an elliptical helix having a c -component significantly smaller than its ab -components [powder : $\mu_{a,b} = 3.53(4)\mu_B$ and $\mu_c = 3.04(5)\mu_B$, single crystal: $\mu_{a,b} = 3.58(11)\mu_B$ and $\mu_c = 3.19(5)\mu_B$]. As illustrated in Fig. 2, all spins lie in a plane perpendicular to the $[1\ 1\ 0]$ direction. Along the c -axis, the spins of iron atoms at $(0\ 0\ \pm z)$ are anti-parallel with those at $(0.5\ 0.5\ 0.5 \pm z)$ [see Fig. 2(a)], which yields the c -component of the propagation vector $k_z = 1$. This helical structure is analogous to those in metallic SrFeO_3 and insulating CaFeO_3 which have a rotation axis of $[1\ 1\ 1]$ [6, 22, 23].

In order to study the dynamical magnetic properties of $\text{Sr}_3\text{Fe}_2\text{O}_7$, we performed INS measurements on a single crystal at $T = 4$ K, well below T_N . Figures 3 (a) and (b) show contour maps of neutron scattering intensities obtained from PUMA up to 14 meV along the $[H00]$ and $[HH0]$ directions, respectively. To quantify the lower-energy excitations more precisely, the spin excitations along the $[HH5]$ direction [Fig. 3 (c)] were measured at the PANDA cold-neutron TAS, where no significant anisotropy gap is observed. In a bilayer system, one typically expects two spin wave branches, optic and acoustic, as observed in high-temperature superconducting cuprates [24] and bilayer manganates [25]. To detect the optical branch, high-energy INS measurements were performed on the MERLIN TOF spectrometer, and the results are summarized in Figs. 3 (d) and (e). We were able to separate the two spin wave branches due to the different dependencies of their INS cross section on the L (c -axis) component of the momentum transfer \vec{q} . The optic (acoustic) branch has maximum cross section when $L\Delta z_{\text{Fe}}$ is half-integer (integer). Here $\Delta z_{\text{Fe}} = 0.195$ is the distance between nearest-neighbor Fe spins within one bilayer, expressed as a fraction of the lattice constant c . The INS signal at $L = 5$, shown in Fig. 3 (d), originates from the acoustic branch. However, the observed strong INS signal, for ~ 22 meV and higher energies [Fig. 3 (e)], at $L = 7$, mostly comes from the optic branch. The optic spin-wave energy gap allowed us to determine the intra-bilayer coupling (J_{c1} in Fig. 2).

As far as low-energy magnon dispersions are concerned, double-exchange systems can be described by spin-only models [26]. Thus, the above physical considerations can be cast into the following phenomenological spin Hamiltonian:

$$H = \sum_{ij} J_{ij} \mathbf{S}_i \cdot \mathbf{S}_j + \Delta \sum_i S_{i\alpha}^2, \quad (1)$$

where J_{ij} represents the Heisenberg coupling between the i -th and j -th spins \mathbf{S} , $\Delta > 0$ is the easy (110) plane anisotropy parameter, and S_α refers to the spin component along the $[110]$ axis.

We have carried out standard linear spin-wave calculations [27], using a minimal set of input parameters in

Eq. (1), to fit the magnon dispersion and intensities observed. In order to describe the main features of the experimental data on a quantitative level, the minimal spin Hamiltonian is found to contain five different exchange couplings. These are the nearest-neighbor J_1 and longer-range J_2, J_3 interactions between Fe-spins within the ab -plane [see Fig. 2(a)], and the c -axis couplings J_{c1} and J_{c3} that stand for the intra- and inter-bilayer interactions, respectively [see Fig. 2(b)]. We have assumed that equivalent domains of the spiral structure contribute equally to the spectra, and convoluted the calculated intensities with the instrumental resolution function. Figures 3(f)-(j) present the results of the calculations with the following parameters: $J_1 = -7.2$ meV, $J_2 = 1.05$ meV, $J_3 = 2.1$ meV, $J_{c1} = -5.1$ meV, $J_{c2} < 0.01$ meV, $J_{c3} = 0.01$ meV, $\Delta = 0.06$ meV. Here positive (negative) values of J correspond to antiferromagnetic (ferromagnetic) interactions. The calculated spin-wave dispersions show a remarkable agreement with the experimental data.

We now turn to the interpretation of our results. The helical order observed and the overall topology of the magnon dispersions are consistent with the negative charge-transfer energy model [10]. However, the predicted extremely soft dispersion ($\sim 10^{-3}$ of the full magnon bandwidth) of spin-waves for \vec{q} values below the ordering vector \vec{k} is inconsistent with the data. As shown in Figs. 3(a)-(c), we observe highly dispersive magnons in the window $\vec{q} < \vec{k}$, reaching a maximum of ~ 3 meV. This is more than an order of magnitude larger than the calculated value of ~ 0.1 meV for a three-dimensional model [10].

In a scenario based on competing ferromagnetic double-exchange and antiferromagnetic superexchange interactions, the balance between both couplings is controlled by the degree of the itineracy/localization of the conduction electrons. The signs and relative strengths of the exchange interactions are consistent with theoretical estimates [2]. Specifically, the strength of the double-exchange coupling $J_{\text{DE}} \simeq -\frac{1}{4S^2}\tilde{t}$, where $\tilde{t} = \kappa t$ with $\kappa < 1$ is the effective hopping amplitude. Enhanced correlations near the metal-insulator transition may considerably reduce the electron mobility and hence the values of κ and J_{DE} . In particular, the choice of $\kappa \sim 0.3$ provides $J_{\text{DE}} \sim -10$ meV which is comparable to typical values of antiferromagnetic superexchange interactions in manganates, $J_{\text{SE}} \sim \frac{1}{4S^2} \frac{t^2}{U} \sim 3$ meV. Whereas spin wave measurements on isostructural manganates [25, 28] are well described by nearest-neighbor exchange Hamiltonians, the longer-range interactions observed in $\text{Sr}_3\text{Fe}_2\text{O}_7$ are consistent with the larger $p-d$ covalency predicted in theoretical work on the iron oxides [2, 10, 11].

A few comments are in order regarding the J values we obtained from the above fits. The large negative values of the nearest-neighbor couplings J_1, J_{c1} imply that ferromagnetic double-exchange in ferrates is sufficiently strong to keep the neighboring spins roughly parallel. (Note that

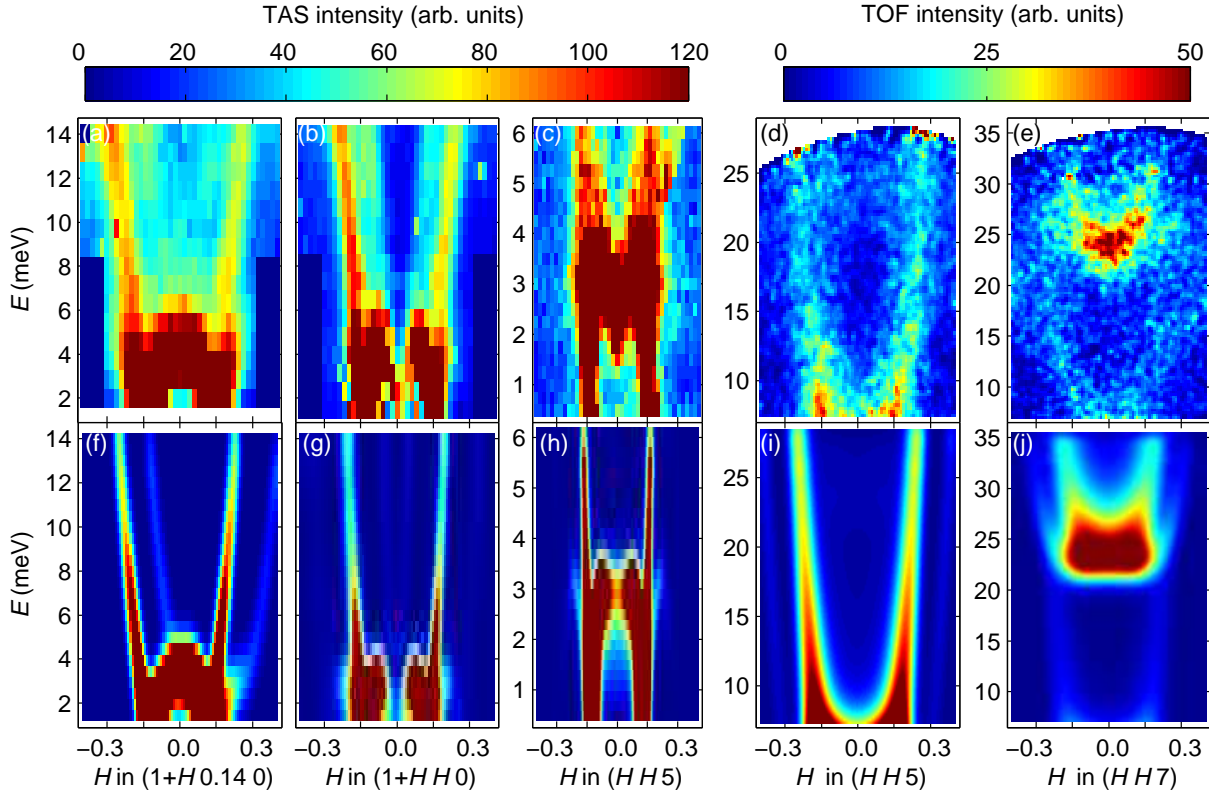


FIG. 3. (Color online) Contour maps of spin-wave dispersions in $\text{Sr}_3\text{Fe}_2\text{O}_7$ at 7 K along the (a) $[H00]$, (b) $[HH0]$, (c-d) $[HH5]$, and (e) $[HH7]$ directions. The intensities in (a) and (b) were multiplied by \sqrt{E} to enhance the upper band. (f)-(j) show the theoretical dispersions and neutron scattering intensities (convoluted with the instrumental resolution), calculated with the parameters described in the text.

$J_1 \sim -|J_{\text{DE}}| + J_{\text{SE}}$.) However, the longer-range antiferromagnetic exchange interactions J_2, J_3 are sizable, and in fact, they are crucial to stabilize the spin-helix against simple ferromagnetic and canted-antiferromagnetic states [29]. A total-energy calculation as a function of wave vector shows that these exchange parameters are compatible with the observed helical spin structure.

Remarkably, the coupling constant J_3 is larger than the second-neighbor interaction J_2 . This can be understood as a consequence of the large $pd\sigma$ virtual charge-transfer along the Fe-O-Fe-O-Fe line. We also note that the ab -plane interaction J_1 is somewhat stronger than the corresponding intra-bilayer c -axis parameter J_{c1} . This suggests the presence of some orbital polarization in favor of the $x^2 - y^2$ state. However, the relatively large ratio of $|J_{c1}/J_1|$ as compared to typical values in the $\text{La}_{2-x}\text{Sr}_x\text{Mn}_2\text{O}_7$ system [25, 28] and in copper oxides with bilayer structure [24] indicates that this polarization is far from complete. On the other hand, $|J_{c1}/J_1|$ is smaller than the one in isostructural $\text{Ca}_3\text{Ru}_2\text{O}_7$ [30], which presumably reflects the different electronic structure of the ruthenates where all $4d^4$ valence electrons reside in the t_{2g} orbitals in a low-spin configuration.

In summary, we have determined the magnetic structure and exchange interactions of $\text{Sr}_3\text{Fe}_2\text{O}_7$, a clean, stoi-

chiometric compound with a quasi-two-dimensional spiral state very close to a MIT. The determination of the spin wave excitations and exchange interactions provides a quantitative confirmation of a decades-old theoretical prediction [3] and a firm experimental basis for further experimental and theoretical work on TMOs near MITs. These include the pseudo-cubic perovskite $\text{Sr}(\text{Fe},\text{Co})\text{O}_{3-\delta}$, which exhibits a rich phase diagram as a function of doping, temperature, and magnetic field [23, 31–34]. It was recently shown that these materials may offer an attractive platform for exploration of skyrmion physics [33, 34]. Analogous studies of $\text{Sr}_3\text{Fe}_2\text{O}_{7-\delta}$ have only recently begun [12]. The excitation spectrum of a clean quasi-two-dimensional spiral we have reported here will also serve as a baseline for comparison to neutron scattering data on magnetically disordered metals near MITs including isostructural $\text{Sr}_3\text{Ru}_2\text{O}_7$, whose spin excitations have been discussed in terms of competing interactions [35], and high-temperature superconducting cuprates, where two-dimensional spiral magnetism is one of the scenarios that has been invoked to explain the unusual incommensurate spin excitations observed in the superconducting state [17, 18].

We thank D. Efremov and C. Ulrich for discussions, the members of the Jansen department and Crystal Growth

service group at MPI-FKF for assistance, and the German Science Foundation (DFG) for financial support under collaborative grant No. SFB/TRR 80.

* b.keimer@fkf.mpg.de

- [1] A. Georges, G. Kotliar, W. Krauth, and M. J. Rozenberg, *Rev. Mod. Phys.* **68**, 13 (1997).
- [2] For a review, see G. Khaliullin, *Prog. Theor. Phys. Suppl.* **160**, 155 (2005).
- [3] P.-G. de Gennes, *Phys. Rev.* **118**, 141 (1960). Note that de Gennes originally predicted canted antiferromagnetism, but longer-range exchange interactions can stabilize spiral magnetism.
- [4] For a review, see E. Dagotto, *Science* **309**, 257 (2005).
- [5] V. Scagnoli, U. Staub, A. M. Mulders, M. Janousch, G. I. Meijer, G. Hammerl, J. M. Tonnerre, and N. Stojic, *Phys. Rev. B* **73**, 100409(R) (2006).
- [6] P. M. Woodward, D. E. Cox, E. Moshopoulou, A. W. Sleight, and S. Morimoto, *Phys. Rev. B* **62**, 844 (2000).
- [7] T. S. Santos, B. J. Kirby, S. Kumar, S. J. May, J. A. Borchers, B. B. Maranville, J. Zarestky, S. G. E. te Velthuis, J. van den Brink, and A. Bhattacharya, *Phys. Rev. Lett.* **107**, 167202 (2011).
- [8] A. Frano, E. Schierle, M. W. Haverkort, Y. Lu, M. Wu, S. Blanco-Canosa, U. Nwankwo, A. V. Boris, P. Wochner, G. Cristiani, H. U. Habermeyer, G. Logvenov, V. Hinkov, E. Benckiser, E. Weschke, and B. Keimer, *Phys. Rev. Lett.* **111**, 106804 (2013).
- [9] S.B. Lee, R. Chen, and L. Balents, *Phys. Rev. B* **84**, 165119 (2011).
- [10] M. Mostovoy, *Phys. Rev. Lett.* **94**, 137205 (2005).
- [11] Z. Li, R. Laskowski, T. Iitaka, and T. Tohyama, *Phys. Rev. B* **85**, 134419 (2012).
- [12] D. C. Peets, J.-H. Kim, P. Dosanjh, M. Reehuis, A. Maljuk, N. Aliouane, C. Ulrich, and B. Keimer, *Phys. Rev. B* **87**, 214410 (2013).
- [13] T. Kimura, Y. Tomioka, H. Kuwahara, A. Asamitsu, M. Tamura, and Y. Tokura, *Science* **274**, 1698 (1996).
- [14] R. A. Borzi, S. A. Grigera, J. Farrell, R. S. Perry, S. J. S. Lister, S. L. Lee, D. A. Tennant, Y. Maeno, and A. P. Mackenzie, *Science* **315**, 214 (2007).
- [15] A. Maljuk, J. Strempfer, C. Ulrich, M. Sofin, L. Capogna, C. T. Lin, and B. Keimer, *J. Cryst. Growth* **273**, 207 (2004).
- [16] For a review, see N. Nagaosa and Y. Tokura, *Nature Nanotech.* **8**, 899 (2013).
- [17] P. A. Lindgard, *Phys. Rev. Lett.* **95**, 217001 (2005).
- [18] A. Lüscher, A.I. Milstein, and O.P. Sushkov, *Phys. Rev. Lett.* **98**, 037001 (2007); *Phys. Rev. B* **75**, 235120 (2007).
- [19] E. E. Rodriguez, C. Stock, P. Zajdel, K. L. Krycka, C. F. Majkrzak, P. Zavalij, and M. A. Green, *Phys. Rev. B* **84**, 064403 (2011).
- [20] T. G. Perring, R. A. Ewings, and J. V. H. Duijn, Horace: visualising and manipulating $S(Q, \omega)$ measured in all four dimensions, <http://horace.isis.rl.ac.uk>.
- [21] J. Rodríguez-Carvajal, *Physica B* **192**, 55 (1993).
- [22] T. Takeda, Y. Yamaguchi, and H. Watanabe, *J. Phys. Soc. Jpn.* **33**, 967 (1972).
- [23] M. Reehuis, C. Ulrich, A. Maljuk, C. Niedermayer, B. Ouladdiaf, A. Hoser, T. Hofmann, and B. Keimer, *Phys. Rev. B* **85**, 184109 (2012).
- [24] J. M. Tranquada, G. Shirane, B. Keimer, S. Shamoto, and M. Sato, *Phys. Rev. B* **40**, 4503 (1989); D. Reznik, P. Bourges, H. F. Fong, L. P. Regnault, J. Bossy, C. Vettier, D. L. Milius, I. A. Aksay, and B. Keimer, *Phys. Rev. B* **53**, 14741(R) (1996).
- [25] T. G. Perring, D. T. Adroja, G. Chaboussant, G. Aeppli, T. Kimura, and Y. Tokura, *Phys. Rev. Lett.* **87**, 217201 (2001).
- [26] G. Khaliullin and R. Kilian, *Phys. Rev. B* **61**, 3494 (2000).
- [27] S. Toth and B. Lake, *arXiv:1402.6069*.
- [28] K. Hirota, S. Ishihara, H. Fujioka, M. Kubota, H. Yoshizawa, Y. Moritomo, Y. Endoh, and S. Maekawa, *Phys. Rev. B* **65**, 064414 (2002).
- [29] N. Shannon and A.V. Chubukov, *Phys. Rev. B* **65**, 104418 (2002).
- [30] X. Ke, Tao Hong, J. Peng, S. E. Nagler, G. E. Granroth, M. D. Lumsden, and Z. Q. Mao, *Phys. Rev. B* **84**, 014422 (2011).
- [31] A. Lebon, P. Adler, C. Bernhard, A.V. Boris, A.V. Pimenov, A. Maljuk, C.T. Lin, C. Ulrich, and B. Keimer, *Phys. Rev. Lett.* **92**, 037202 (2004).
- [32] P. Adler, A. Lebon, V. Damjanovic, C. Ulrich, C. Bernhard, A. V. Boris, A. Maljuk, C. T. Lin, and B. Keimer, *Phys. Rev. B* **73**, 094451 (2006).
- [33] S. Ishiwata, M. Tokunaga, Y. Kaneko, D. Okuyama, Y. Tokunaga, S. Wakimoto, K. Kakurai, T. Arima, Y. Taguchi, and Y. Tokura, *Phys. Rev. B* **84**, 054427 (2011).
- [34] S. Chakraverty, T. Matsuda, H. Wadati, J. Okamoto, Y. Yamasaki, H. Nakao, Y. Murakami, S. Ishiwata, M. Kawasaki, Y. Taguchi, Y. Tokura, and H. Y. Hwang, *Phys. Rev. B* **88**, 220405 (2013).
- [35] L. Capogna, E. M. Forgan, S. M. Hayden, A. Wildes, J. A. Duffy, A. P. Mackenzie, R. S. Perry, S. Ikeda, Y. Maeno, and S. P. Brown, *Phys. Rev. B* **67**, 012504 (2003).